Targeting Highly Reactive Labile Magnesium in Ultramafic Tailings for Greenhouse-Gas Offsets and Potential Tailings Stabilization at the Baptiste Deposit, Central British Columbia (NTS 093K/13, 14)

S.S.S. Vanderzee, Bradshaw Research Initiative for Minerals and Mining, The University of British Columbia, Vancouver, BC, svander@eoas.ubc.ca

G.M. Dipple, Bradshaw Research Initiative for Minerals and Mining, The University of British Columbia, Vancouver, BC

P.M.D. Bradshaw, FPX Nickel Corp., Vancouver, BC

Vanderzee, S.S.S., Dipple, G.M. and Bradshaw, P.M.D. (2019): Targeting highly reactive labile magnesium in ultramafic tailings for greenhouse-gas offsets and potential tailings stabilization at the Baptiste deposit, central British Columbia (NTS 093K/13, 14); *in* Geoscience BC Summary of Activities 2018: Minerals and Mining, Geoscience BC, Report 2019-1, p. 109–118.

Introduction

The products of mining are essential for modern society, the renewable energy infrastructure and transportation systems of the future; however, their recovery produces an enormous volume of solid waste and is a significant contributor to anthropogenic greenhouse-gas emissions. The amount of mine waste produced worldwide is on the same order of magnitude as that of natural Earth-shaping erosional processes: some tens of billions of tonnes of waste per year (Fyfe, 1981; Förstner, 1999; Blight, 2011), most of which consists of tailings (Kossoff et al., 2014). Mine tailings (pulverized rock that remains after the extraction of economic metals and minerals) are often disposed of within dammed impoundments called tailings storage facilities. The physical stability of mine tailings is important because the failure of the impoundment walls can result in the release of large volumes of waste, which can cause significant environmental and economic damage, and in some cases, loss of human life (do Carmo et al., 2017). The focus of this paper is achieving optimal management of mine tailings and reducing greenhouse-gas (GHG) emissions, which is important to the sustainability of extractive industries and society as a whole (Intergovernmental Panel on Climate Change, 2014; Kossoff et al., 2014).

One method for stabilizing mine tailings suggested by Choi et al. (2009) is the addition of binders such as Portland cement. Choi et al. (2009) found that a Portland cement content of 5 wt. % was sufficient to stabilize the tailings and satisfy unconfined compressive strength guidelines of 0.35 MPa (50 psi.), which is generally accepted to represent stabilized waste that can withstand overburden pressures in a landfill (LaGrega et al., 1994). This approach would, however, increase a mine's carbon footprint because approximately 800 kg of CO_2 is produced by manufacturing 1 t of Portland cement (Worrell et al., 2001). It would also add significant costs because Portland cement is approximately US$100/t (Statista, 2018); therefore, 5 wt. % consumption per tonne of tailings would add $5/t to the mining costs.

For mines that produce ultramafic tailings, an attractive and potentially cost-effective option is to promote the sequestration of CO_2 in the tailings, which has the potential to promote stabilization by the formation of cementitious secondary magnesium carbonate minerals within the tailings after they are deposited. This can be accomplished through the exposure of the tailings to atmospheric CO_2 and/or concentrated CO_2 steam such as flue gas. This results in the alteration of magnesium hydroxide minerals (e.g., brucite $\{Mg(OH)_2\}$ and hydrotalcite-group minerals such as iowaite $\{Mg_6Fe_2(OH)_{16}Cl_2 \cdot H_2O\}$) that are typically present in trace abundance in ultramafic tailings (Wilson et al., 2014) along with the more abundant magnesium silicate minerals (e.g., serpentine $\{Mg_3Si_2O_5(OH)_4\}$). During the process, termed carbon mineralization, magnesium ions (Mg^{2+}) are released into the pore water of the tailings where they can then react with dissolved CO_2 species such as HCO_3^- to precipitate magnesium carbonate minerals such as nesquehonite $\{MgCO_3 \cdot 3H_2O\}$, dypingite $\{Mg_5(CO_3)_4(OH)_2 \cdot 5H_2O\}$ and hydromagnesite ($\{Mg_5(CO_3)_4(OH)_2 \cdot 4H_2O\}$; Wilson et al., 2014). These reactions effectively turn the CO_2 gas into an environmentally benign mineral. The most economically viable method to accelerate these reactions is likely to target tailings that contain enriched levels of highly reactive labile magnesium so that energy- and chemical-intensive acceleration technologies are not required to overcome the relatively slow bulk dissolution rates of magnesium silicate minerals (Daval et al., 2013).

This publication is also available, free of charge, as colour digital files in Adobe Acrobat® PDF format from the Geoscience BC website: http://www.geosciencebc.com/s/SummaryofActivities.asp.

The authors define labile magnesium as being sourced from highly reactive hydroxide minerals—brucite and hydrotalcites—and from the surface of serpentine, where the very outer layers of the sheet silicate will readily release their magnesium ions but the bulk of the mineral grain will not (Thom et al., 2013). Based on Thom et al. (2013), Harrison et al. (2015) and our preliminary flow-through dissolution experiments, this paper considers 100% of the magnesium in brucite and hydrotalcites to be labile and 2.5% of the magnesium in serpentine to be labile. The labile magnesium ions are much more rapidly released into the pore water of tailings at atmospheric temperature and pressure; therefore, secondary magnesium carbonate cement can be readily produced at low cost and within a relatively short time frame. In the case of the Mount Keith nickel mine in Western Australia, 11% of annual CO_2 emissions were unintentionally offset due to the uptake of CO_2 from the atmosphere by labile magnesium–bearing tailings without any additional costs, and reactive transport models infer that small changes in tailings management practices could allow the labile magnesium to fully react and offset up to 60% of the mine's emissions (Wilson et al., 2014).

A problem with using this process at a mine site to stabilize tailings and significantly offset greenhouse-gas emissions is that the labile magnesium content within a single mineral deposit, and therefore within mine tailings, is highly variable due to the inherent geological variability. The abundance and spatial distribution of labile magnesium throughout a mineral deposit can be inferred by measuring mineral abundance in exploration drillcore through Rietveld X-ray diffraction; however, this technique is time and cost intensive and is not practical for mine planning reconnaissance studies that can require a mineral abundance analysis of several tens of thousands of samples. Alternatively, the problem can be solved by using estimations of mineral abundance that can be rapidly and inexpensively computed from whole-rock analytical data that are routinely collected on drillcore during exploration. In this paper, the authors apply the projection method of computing mineral abundance (Thompson, 1982; Gordon and Dipple, 1999) to the whole-rock analytical data from exploration drillcore from the Baptiste nickel deposit (MINFILE 093K 116; BC Geological Survey, 2018), which is part of the Decar nickel district in central British Columbia (BC). This deposit is unique in that the nickel is hosted within a highly magnetic and dense nickel-iron alloy called awaruite (Britten, 2017; Milidragovic et al., 2018). The mineral abundance computations are used to estimate the labile magnesium content of the Baptiste nickel deposit, and therefore, the carbon sequestration potential. This allows the spatial distribution of the labile magnesium to be mapped and the enriched zones to be targeted for the creation of cemented and stabilized tailings impoundment walls. If successful at a mine operating scale, this could reduce the cost of tailings storage as well as the magnitude of environmental risk.

Methods

Whole-Rock Chemical Compositions

The whole-rock chemical composition of 9990 exploration drillcore pulps from the Baptiste nickel deposit were determined by four-acid digestion followed by inductively coupled plasma–optical emission spectrometry (ICP-OES) analysis and were supplied by FPX Nickel Corp. These data were reduced to 7604 samples by removing samples labeled as wasterock (2323 samples) and dikes (63 samples). Included in these data are measurements of loss on ignition (LOI), which can be derived from the volatilization of H_2O from hydroxyl within brucite and serpentine, CO_2 from carbonate minerals and SO_2 following the oxidation of sulphide minerals during ignition. It is assumed that the LOI is derived solely from H_2O loss because carbonate-bearing rock types such as listwanite (which is composed of magnesite and quartz and is not a source of labile magnesium) were removed from the dataset by the wasterock query filter, and the sulphur content of the Baptiste samples was negligible (mean of 0.02 wt. %). The major-element composition for the test set of 30 samples with high MgO that was used for model calibration and validation is shown in Table 1.

Rietveld X-ray Diffraction

In this paper, Rietveld X-ray diffraction (R-XRD) data on 10 samples were used to determine the model minerals, which are minerals that are characteristic of the deposit—or at least characteristic of specific zones of interest within the deposit—and to calibrate the mineral abundance computation model. An additional 20 samples were used to validate the computations of the model. The samples analyzed by R-XRD were course rejects from exploration pulps and were prepared for XRD analysis by first reducing the material's particle size in a steel ring mill for 5 minutes. The material was then further pulverized as an ethanol slurry in a vibratory McCrone micronizing mill for 7 minutes (Wilson et al., 2006). The R-XRD results are shown in Table 2.

Computing Mineral Abundance from Whole-Rock Elemental Compositions

A mass balance relationship is used to determine what proportion of the model minerals best explains the whole-rock chemical assay data. There must be a mass balance for each of the *m* constituents (commonly the oxides that represent most of the rock) of the analyses with the computed model mineral abundances *n*. These mass balances can be expressed as follows:

$$\sum_{j=1}^{n} a_{ij} x_j = b_i \qquad \begin{matrix} i = 1,2,\ldots m \\ j = 1,2,\ldots m \end{matrix} \qquad (1)$$

where a_{ij} represents the amount of constituent i in mineral j, b_i represents the amounts of constituent i in the whole-rock chemical composition and x_j represents the unknown abundance of model minerals. In this approach, exchange components are allowed for (Thompson, 1982), which in this paper allows Fe^{2+} to substitute for Mg^{2+} ($FeMg_{-1}$) and $Fe^{3+}Al^{3+}$ to substitute for $Fe^{2+}Si^{4+}$ ($AlSi_{-1}$) within minerals to an extent that best fits the projected mineral abundance to the whole-rock chemical assay data, and allows each sample to have a unique computed mineral composition.

The computations were performed in MATLAB by describing the mass balance equation (equation 1) as the system of equations shown below. Based on the R-XRD data in Table 2, brucite {$Mg(OH)_2$}, magnetite {Fe_3O_4}, forsterite {Mg_2SiO_4}, serpentine {$Mg_3Si_2O_5(OH)_4$} and diopside {$CaMgSi_2O_6$} were used as model minerals to explain the whole-rock chemical assay data; however, the addition of the $FeMg_{-1}$ exchange component introduces an unknown into the computation formula without adding an equation because no new major chemical constituents are introduced. As a result, if all the model minerals identified in Table 2 were retained in addition to the exchange components, the system would become underdetermined and a unique solution for mineral abundance would not be obtainable. This necessitates the removal of one of the model minerals so that the number of unknowns will equal the number of equations. Magnetite was selected for removal because the R-XRD and whole-rock composition assay data showed that the magnetite abundance was not proportional to the total amount of Fe in the sample, and the measured abundance in the 10 calibration samples showed a relatively low degree of variability (~1–5 wt. % magnetite). A constant magnetite abundance of 3.8 wt. % was assumed in all samples, which was estimated based on petrographic and geochemical data. Now that the model minerals, their constituents (Table 1) and exchange components have been identified, the system of equations can be described in matrix form, as seen in Figure 1.

The projection model was then empirically refined based on the quantitative R-XRD data by adjusting a series of parameters (serpentine composition and the percentage of LOI associated with the dihydroxylation of serpentine and

Table 1. Major-element chemical composition of the test set of 30 samples with high MgO used for model calibration validation. Abbreviation: LOI, loss on ignition.

Sample code	Fe_2O_3 (wt. %)	MgO (wt. %)	CaO (wt. %)	SiO_2 (wt. %)	Al_2O_3	LOI	Total
Model calibration samples							
1423082	7.81	43.07	0.04	33.74	0.06	14.21	98.93
1423072	7.9	42.85	0.02	34.65	0.15	14.73	100.3
1423092	7.97	42.89	0.09	35.41	0.06	13.97	100.39
1423128	7.02	42.39	0.05	37.35	0.21	12.71	99.73
1423127	7.88	42.52	0.1	36.05	0.4	12.74	99.69
1423090	8.07	39.65	0.47	37.1	1.12	12.66	99.07
1423106	7.37	40.68	0.2	38.95	0.82	12.28	100.3
1423149	8.39	40.83	0.54	37.99	0.84	11.68	100.27
1423108	7.36	37.39	1.5	38.99	1.86	11.56	98.66
1423111	8.32	37.69	0.86	39.45	1.75	11.51	99.58
Model validation samples							
1423073	7.62	41.93	0.01	35.72	0.08	14.19	99.55
1423078	7.84	43.12	0.03	36.45	0.29	12.18	99.91
1423079	8.18	42.41	0.03	35.03	0.19	14.25	100.09
1423083	7.77	42.57	0.03	34.9	0.06	14.48	99.81
1423084	7.22	42.27	0.01	33.67	0.06	14.08	97.31
1423086	7.87	42.15	0.01	34.41	0.12	14.05	98.61
1423088	7.63	42.47	0.02	35.39	0.24	12.83	98.58
1423091	7.48	41.41	0.03	34.28	0.12	14.01	97.33
1423094	7.63	42.51	0.01	33.81	0.06	14.28	98.3
1423096	6.64	43.09	0.02	35.69	0.18	13.45	99.07
1423116	7.96	37.13	0.85	39.19	1.48	11.96	98.57
1423117	8.49	38.34	0.75	38.81	1.36	12.33	100.08
1423118	8.26	36.99	1.13	38.55	1.7	12.02	98.65
1423134	7.69	40.86	0.26	36.47	0.72	12.99	98.99
1423132	8.47	40.66	0.14	37.22	0.89	13.09	100.47
1423162	7.64	38.3	0.82	38.5	1.46	12.28	99
1423167	7.84	38.22	1.43	37.74	1.07	12.49	98.79
1423178	8.19	38.14	1.71	39	1.21	12.32	100.57
1423188	7.98	38.7	1.48	39.19	1.29	11.98	100.62
1423189	7.87	39	1.58	38.87	1.25	11.99	100.56

Table 2. Results of Rietveld X-ray diffraction refinement on course rejects of exploration pulps.

Sample code	Brucite (wt. %)	Magnetite (wt. %)	Forsterite (wt. %)	Serpentine (wt. %)	Diopside (wt. %)
Model calibration samples					
1423082	12.61	3.55	4.79	78.4	0.66
1423072	10.12	4.08	3.44	81.84	0.52
1423092	9.79	2.48	2.95	83.52	1.26
1423128	6.77	3.57	8.33	81.33	0
1423127	4.58	2.2	11.56	81.65	0
1423090	1.84	1.82	10.95	84.56	0.83
1423106	1.44	1.65	11.04	85.61	0.25
1423149	1.15	1.32	17.6	78.97	0.96
1423108	0.53	3.09	5.88	87.51	2.99
1423111	0.24	4.6	3.92	88.88	2.37
Model validation samples					
1423073	10.68	5.94	3	79.85	0.53
1423078	5.8	1.98	20.5	71.42	0.3
1423079	9.62	3.42	6.42	80.11	0.43
1423083	12.19	4.79	3.52	78.95	0.56
1423084	12.57	6.46	4.19	76.28	0.5
1423086	10.78	4.5	5.48	78.87	0.37
1423088	7.46	3	13.32	76.19	0.01
1423091	10.81	6.71	4.52	77.69	0.28
1423094	10.74	2.8	3.46	82.25	0.73
1423096	9.58	4.29	7.42	78.3	0.41
1423116	0.56	4.17	2.74	90.44	2.08
1423117	0.68	3.43	4.21	90.07	1.59
1423118	0.29	3.12	5.32	89.59	1.68
1423134	4.97	3.1	7.27	83.92	0.73
1423132	1.82	2.69	4.43	90	1.06
1423162	0.74	2.66	7.78	87.14	1.7
1423167	1.09	1.54	10.47	84.45	2.45
1423178	0.78	2.78	4.93	88.1	3.43
1423188	0.77	2.73	8.92	84.6	2.99
1423189	0.89	2.39	9.51	83.9	3.17

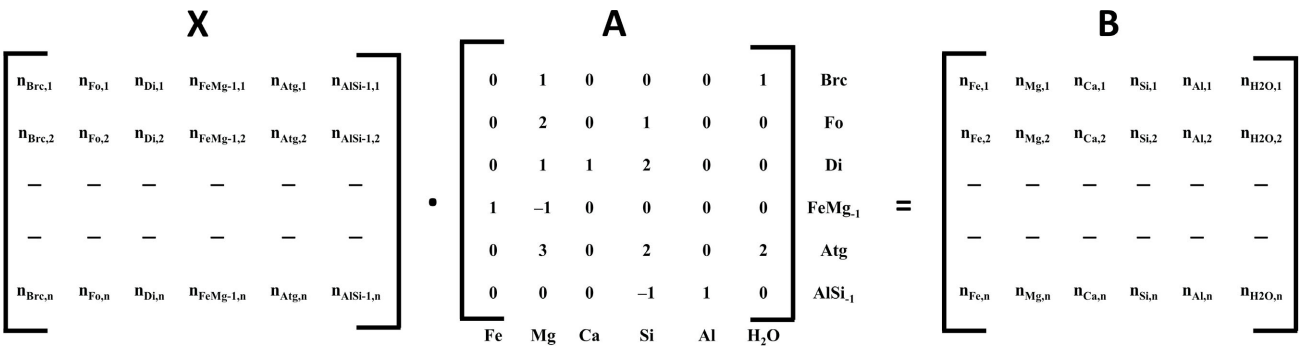

Figure 1. System of equations used to compute mineral abundances within the Baptiste nickel deposit, where the 'X' matrix is the unknown and defines the number of moles of each model mineral or exchange component per 100 g of material, with column dimensions defined by the number of model minerals plus the number of exchange components, and row dimensions by the number of samples (n). The 'A' matrix represents the molar stoichiometry of each model mineral and exchange component. As shown by the labels adjacent to the A matrix, the column dimensions are defined by the major chemical constituents (e.g., Fe, Mg, H_2O) and the row dimensions are defined by the model minerals and exchange components. Lastly, the 'B' matrix defines the number of moles of each chemical component per 100 g of material, with column dimensions defined by the number of major chemical components and row dimensions defined by the number of samples (n). The values in the B matrix are obtained by converting whole-rock geochemical assay data (Table 1) from weight percent oxide to molar concentrations. Abbreviations: Atg, antigorite; Brc, brucite; Di, diopside; Fo, forsterite.

brucite) through a least squares approach. The serpentine composition was refined so that the magnesium to silicon ratio was 1.57 to 1.0, and the LOI was adjusted by a factor of 0.96 to reflect structurally bound water. The mineral abundance computation model was refined based on R-XRD results for 10 samples and 20 additional samples were used to verify the computations of the model.

Results

Brucite and serpentine are the predominant sources of labile magnesium in the Baptiste nickel deposit. Accurate estimation of their abundance is therefore important for estimating labile magnesium abundance. A comparison between the measured and computed abundance of brucite is shown in Figure 2. The first 10 samples were used to calibrate the projection model and an additional 20 samples were analyzed after the projection model was built to test its accuracy. Figure 2 shows that the projection model could provide useful mineralogical computations with an average difference between the measured and computed brucite abundance of –0.1 wt. % and a standard deviation of 1.1 wt. %. Where the projection model produced negative computed brucite abundances (1477 samples out of 7604), the values were set to zero and might be explained by the presence of trace or amorphous minerals that were not included as model minerals.

Figure 3 shows the comparisons between the measured and computed abundances of all the model minerals that were included in the projection model and shows that the projection model also has strong predictive capability for serpentine content, which is important because the mineral surfaces of serpentine are also a significant source of labile magnesium. The forsterite and diopside computations are significantly less reliable; however, this is not important because forsterite and diopside do not contribute a significant amount of labile magnesium (or calcium) to mine tailings because of low reactive surface area density and slow dissolution kinetics, respectively.

The projection model was then applied to all 7604 whole-rock assays from the Baptiste deposit to assess the mineralogical heterogeneity, the labile magnesium content as a measure of the carbon sequestration capacity and the fraction and location of future tailings material that has sufficient labile magnesium to potentially stabilize the tailings through carbon mineralization. Histograms of computed brucite and serpentine content within the Baptiste deposit are shown in Figure 4. Although more than 25% of the deposit is computed to have no brucite, 75% contains brucite ranging from trace amounts to in excess of 10%. Serpentine dominates the mineralogy of all samples.

Implications

Labile magnesium content estimated from computed mineral content is plotted as weight percent MgO in Figure 5. This provides a preliminary assessment of the carbon sequestration capacity of mine tailings. To estimate greenhouse-gas emissions from mine operations production data from the Mount Keith nickel mine in Western Australia, a serpentinite-hosted nickel deposit was used. At Mount Keith, natural gas is used to generate electricity for the ore processing facility (which accounted for ~66% of their CO_2 emissions) and diesel-powered mining haul trucks account for the remaining ~34% (WMC Resources Ltd., 2002). In total, the mine produced 33.6 t CO_2/kt rock mined (Wilson et al., 2014); therefore, mines that use hydroelectric power still need to sequester 11.4 t CO_2/kt rock mined to be GHG neutral due to emissions from the haul truck fleet. From these data, it can be estimated that an average of 1.3 wt. %

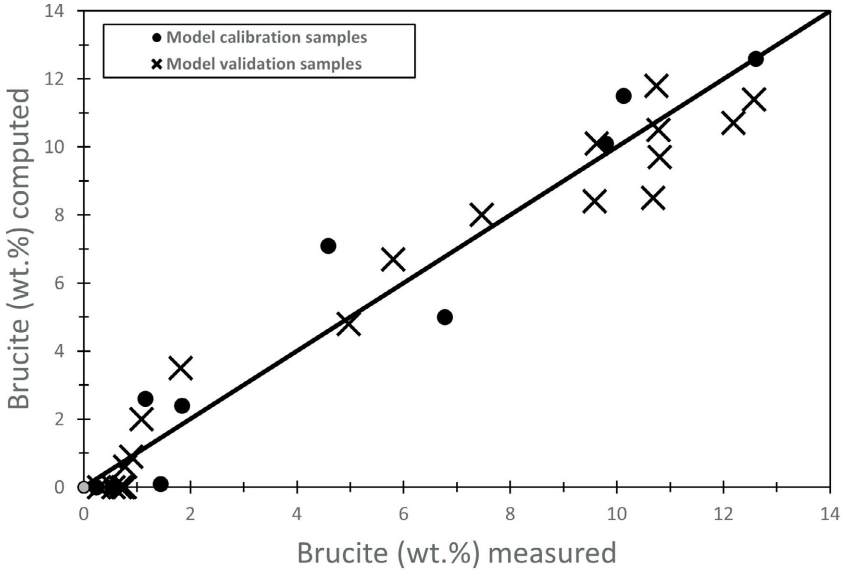

Figure 2. Abundance of brucite computed by the projection model versus the brucite abundance measured by Rietveld X-ray diffraction.

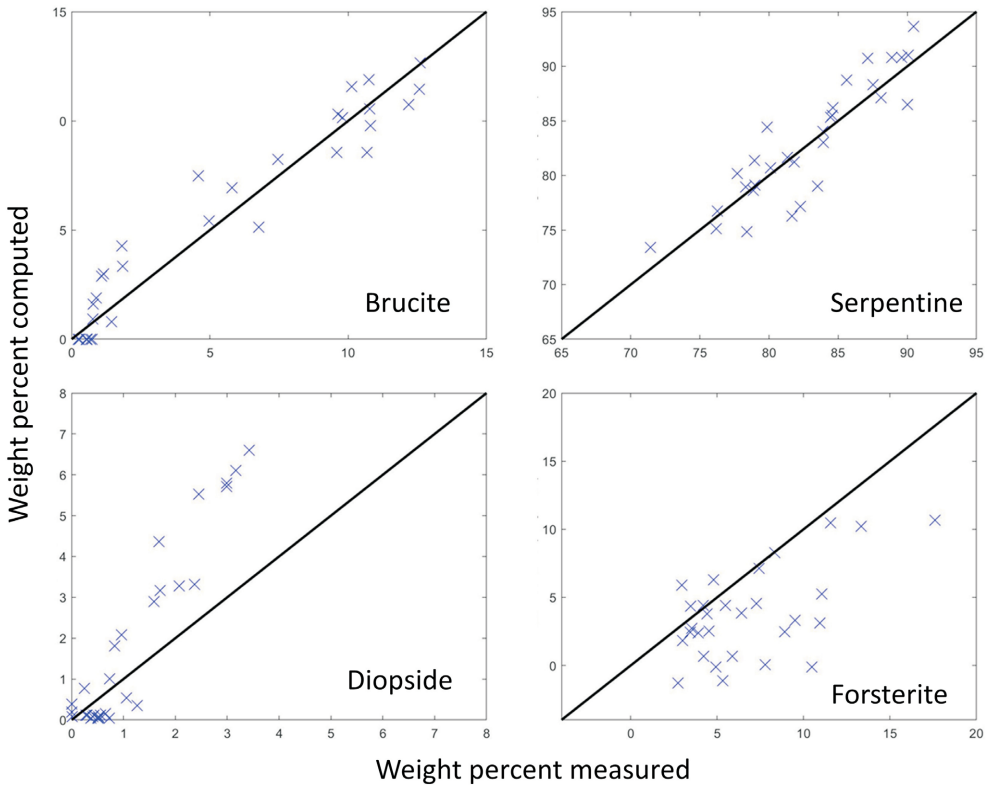

Figure 3. Mineral abundance for brucite and three other minerals computed by the projection model versus the mineral abundance measured by Rietveld X-ray diffraction.

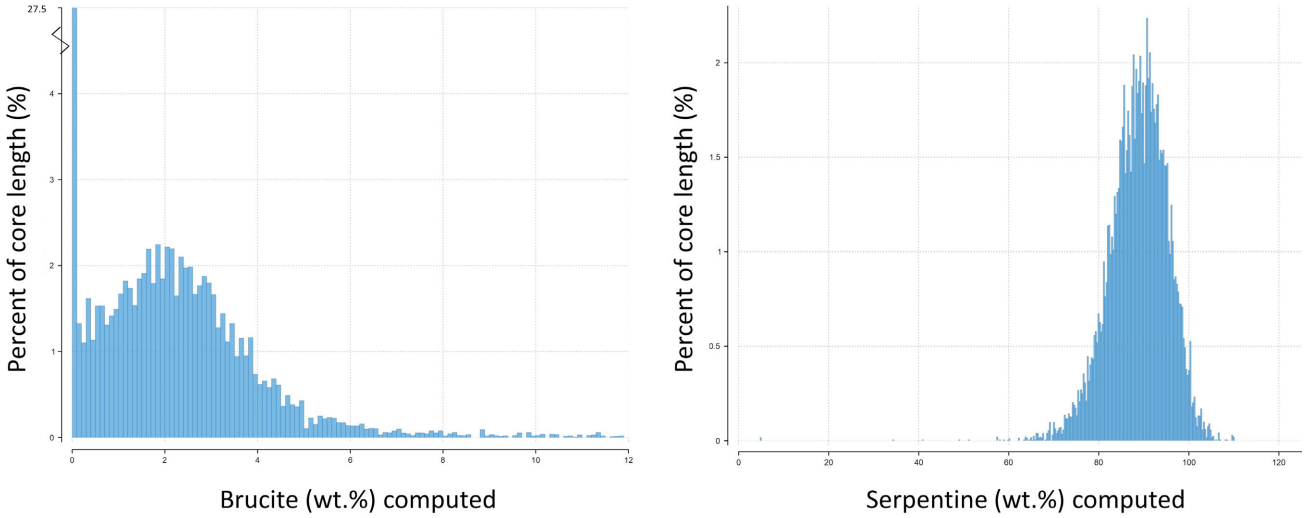

Figure 4. Abundance of brucite and serpentine computed by the projection model across the Baptiste nickel deposit. Samples described as wasterock or dikes in the geochemistry dataset were omitted. The mean brucite and serpentine content is 1.8 wt. % and 88.8 wt. % respectively.

labile MgO is sufficient to make an open-pit nickel mine carbon neutral assuming hydroelectricity is used, and 3.9 wt. % labile MgO if natural gas is used for electricity generation. The Baptiste nickel mine is located near hydroelectric infrastructure; therefore, an estimated average of 1.3 wt. % labile MgO would provide sufficient capacity for carbon-neutral mining. Figure 5 shows that the projection model computations give an average labile magnesium content of 2.3 wt. %. This suggests that the Baptiste mine has more than enough carbon sequestration capacity from labile magnesium to become a carbon neutral mine. Figure 6 shows that if carbon mineralization efforts are focused on the most labile magnesium–rich tailings, only 30% of the tailings need to react with CO_2 to make the Baptiste mine carbon neutral over its lifetime. In addition, this same labile magnesium–rich 30% fraction of the tail-

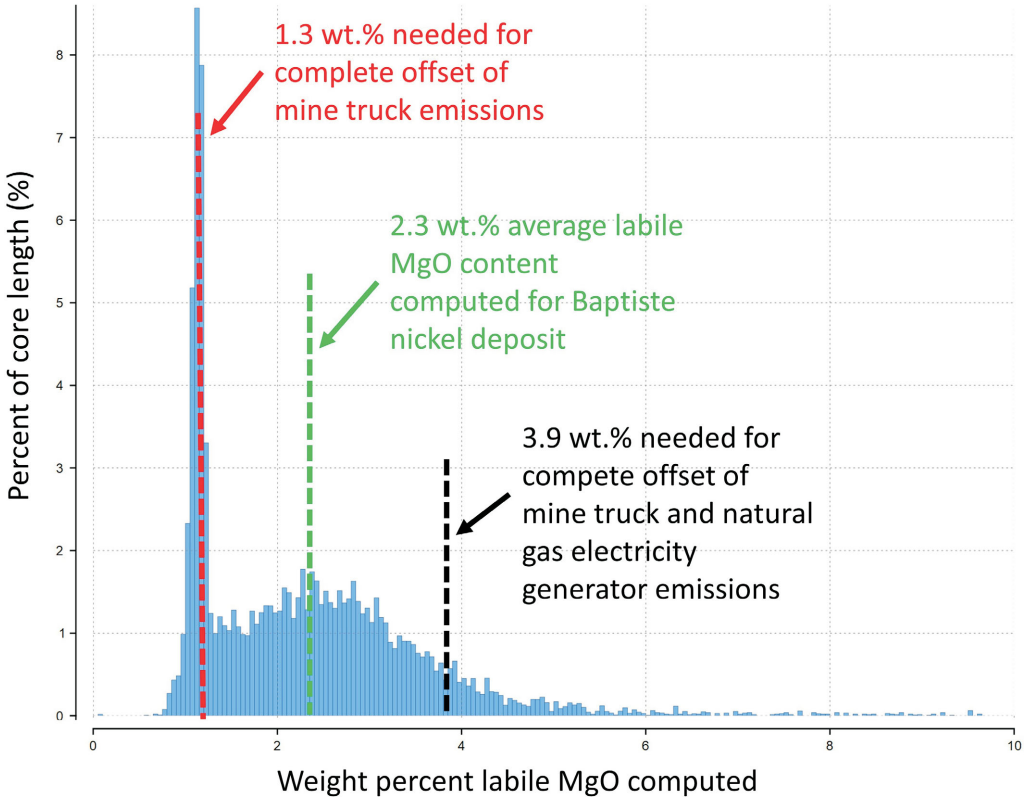

Figure 5. Histogram of the computed labile magnesium content of drillcore from the Baptiste nickel deposit.

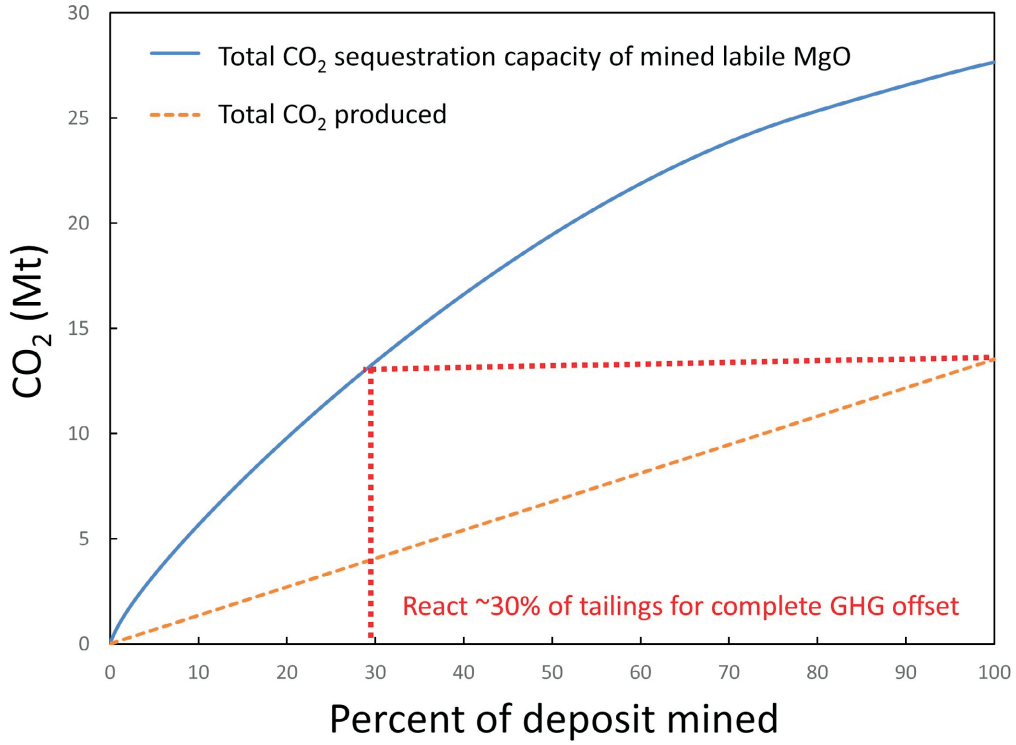

Figure 6. Anticipated CO_2 emissions from nickel mining as a function of the percentage of the deposit that has been mined. The authors assume 1.8 Gt of rock will be mined because this represents the indicated reserve of the Baptiste deposit (FPX Nickel Corp., 2018). The solid line shows the potential rate of carbon sequestration if the most labile magnesium–rich (MgO) zones are used first. Hydroelectricity is assumed for computed complete greenhouse-gas (GHG) offset.

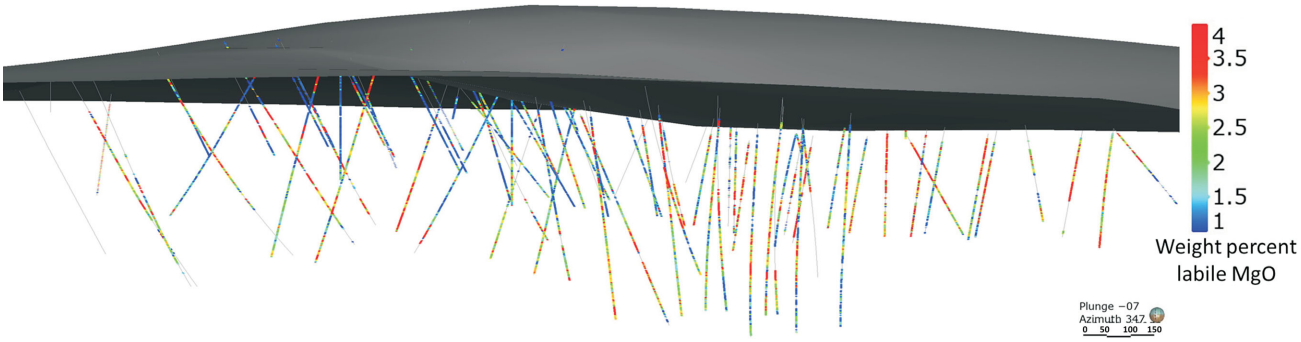

Figure 7. Computed labile magnesium (in wt. % MgO) in mineralized drillcore sections of the Baptiste nickel deposit, central British Columbia. Wasterock sections are shown in grey and were excluded from labile magnesium computations.

ings has the potential to become stabilized by the formation of magnesium carbonate cement, as indicated by lab-scale tests that showed that tailings with approximately 3 wt. % brucite or more can achieve unconfined compressive strengths of approximately 4137 kPa (600 psi.) to more than 5516 kPa (800 psi.) after sequestering 10% CO_2 for two weeks (Vanderzee et al., 2018).

These results may be typical of serpentinite-hosted nickel deposits. For example, carbon mineralization in tailings of the Mount Keith nickel mine has been documented (Wilson et al., 2014) and the potential at the Dumont nickel mine in Quebec is being explored (Kandji et al., 2017). To help target the labile magnesium–rich areas of mineral deposits for carbon mineralization purposes, the authors propose using exploration geochemical data to make mineral abundance computations so that 3-D maps of labile magnesium (Figure 7) can be incorporated into the mine plan.

Conclusions and Future Work

This study, in combination with Vanderzee et al. (2018), has demonstrated at the lab scale that the Baptiste mine likely contains enough labile magnesium to potentially sequester all the CO_2 produced by its mining trucks (11.4 t CO_2/kt rock mined). This would make Baptiste GHG neutral if it used hydroelectric power, which is likely to be the case in BC, and may stabilize the tailings at the same time. To improve, or at least complement, the accuracy of the labile magnesium estimations, other methods of computing mineral abundance can be applied to Baptiste. These methods include linear programming (Gordon and Dipple, 1999), phase equilibria (Connolly, 2005) and MINSQ (Herrmann and Berry, 2002). Furthermore, the authors' laboratory work on tailings stabilization has been very encouraging and the next steps include investigating methods to further accelerate the reaction rates by promoting the transport of CO_2 into the tailings and conducting larger field-scale experiments. These experiments will include measurements of CO_2 sequestration rates, stabilization tests and reactive transport modelling. If the laboratory work can be verified at the field scale, Baptiste could be revolutionary for tailings management and climate change mitigation efforts, as well as for being the first awaruite deposit in the world to be mined.

Acknowledgments

In addition to Geoscience BC, the authors acknowledge FPX Nickel Corp. and the Natural Sciences and Engineering Research Council for financial support of this project. The authors also thank D. Milidragovic from the BC Geological Survey for reviewing this paper.

References

BC Geological Survey (2018): MINFILE BC mineral deposits database; BC Ministry of Energy, Mines and Petroleum Resources, BC Geological Survey, URL <http://minfile.ca/> [November 2018].

Blight, G. (2011): Mine waste: a brief overview of origins, quantities and methods of storage; *in* Waste: A Handbook for Management, p. 77–88.

Britten, R. (2017): Regional metallogeny and genesis of a new deposit type-disseminated awaruite (Ni_3Fe) mineralization hosted in the Cache Creek terrane; Economic Geology, v. 112, p. 517–550.

do Carmo, F.F., Kamino, L.H.Y., Junior, R.T., de Campos, I.C., de Carmo, F.F., Silvino, G., da Silva, K.J., de Castro, X., Mauro, M.L., Rodrigues, N.U.A., de Souza Miranda, M.P. and Pinto, C.E.F. (2017): Fundão tailings dam failures: the environment tragedy of the largest technological disaster of Brazilian mining in global context; Perspectives in Ecology and Conservation, v. 15, no. 3, p. 145–151.

Choi, W.H., Lee, S.R. and Park, J.Y. (2009): Cement based solidification/stabilization of arsenic-contaminated mine tailings; Waste Management, v. 29, no. 5, p. 1766–1771.

Connolly, J.A.D. (2005): Computation of phase equilibria by linear programming: a tool for geodynamic modeling and its application to subduction zone decarbonation; Earth and Planetary Science Letters, v. 236, p. 524–541.

Daval, D., Hellmann, R., Martinez, I., Gangloff, S. and Guyot, F. (2013): Lizardite serpentine dissolution kinetics as a function of pH and temperature, including effects of elevated pCO_2; Chemical Geology, v. 351, p. 245–256.

Dipple, G.M., Raudsepp, M. and Gordon, T.M. (2001): Assaying wollastonite in skarn; *in* CIM Special Volume: Industrial Minerals in Canada, p. 1–10.

Förstner, U. (1999): Introduction; *in* Environmental Impacts of Mining Activities: Emphasis on Mitigation and Remedial Measures, Springer, Heidelberg, p. 1–3.

FPX Nickel Corp. (2018): Developing Canada's next nickel district; FPX Nickel Corp., URL <https://fpxnickel.com/wp-content/uploads/2017/08/FPX-Nickel-Corporate-Presentation.pdf> [November 2018].

Fyfe, W. (1981): The environmental crisis: quantifying geosphere interactions; Science, v. 213, p. 105–110.

Gordon. T.M. and Dipple, G.M. (1999): Measuring mineral abundance in skarn. II. A new linear programming formulation and comparison with projection and Rietveld methods; The Canadian Mineralogist, v. 37, p. 17–26.

Harrison, A.L., Dipple, G.M., Power, I.M. and Mayer, K.U. (2015): Influence of surface passivation and water content on mineral reactions in unsaturated porous media: implications for brucite carbonation and CO_2 sequestration; Geochimica et Cosmochimica Acta, v. 148, p. 477–495.

Herrmann, W. and Berry, R.F. (2002): MINSQ – a least squares spreadsheet method for calculating mineral proportions from whole rock major element analyses; Geochemistry: Exploration, Environment, Analysis, v. 2, no. 4, p. 361–368.

International Panel on Climate Change (2014): Summary for policymakers; *in* Climate Change 2014: Impacts, Adaptation, and Vulnerability, Part A: Global and Sectoral Aspects, Contribution of Working Group II to the Fifth Assessment Report of the Intergovernmental Panel on Climate Change. C.B. Field, V.R. Barros, D.J. Dokken, K.J. Mach, M.D. Mastrandrea, T.E. Bilir, M. Chatterjee, K.L. Ebi, Y.O. Estrada, R.C. Genova, B. Girma, E.S. Kissel, A.N. Levy, S. MacCracken, P.R. Mastrandrea and L.L.White (ed.), Cambridge University Press, Cambridge, UK, p. 1–32.

Kandji, E.H., Plante, B., Bussière, B., Beaudoin, G. and Dupont, P.P. (2017): Geochemical behavior of ultramafic waste rocks with carbon sequestration potential: a case study of the Dumont Nickel Project, Amos, Québec; Environmental Science and Pollution Research, v. 24, p. 11734–11751, URL <https://doi.org/10.1007/S11356-017-8735-9> [November 2018].

Kossoff, D., Dubbin, W.E., Alfredsson, M., Edwards, S.J., Macklin, M.G. and Hudson-Edwards, K. (2014): Mine tailings dams: characteristics, failure, environmental impacts, and remediation; Applied Geochemistry, v. 51, p. 229–245.

LaGrega, M.D., Buckingham, P.L. and Evans, J.C. (1994): Hazardous Waste Management; McGraw-Hill Inc., New York, 1202 p.

Milidragovic, D., Grundy, R. and Schiarizza, P. (2018): Geology of the Decar area north of Trembleur Lake, NTS 93K/14; *in* Geological Fieldwork 2017, BC Ministry of Energy, Mines and Petroleum Resources, BC Geological Survey, Paper 2018-1, p. 129–142.

Statista (2018): Cement prices in the United States from 2007 to 2017; URL <https://www.statista.com/statistics/219339/us-prices-of-cement/> [November 2018].

Thompson, J.B., Jr. (1982): Reaction space: an algebraic and geometric approach; *in* Characterization of Metamorphism through Mineral Equilibria; Reviews in Mineralogy and Geochemistry, v. 10, p. 33–52.

Thom, J.G.M., Dipple. G.M., Power, I.M. and Harrison, A.L. (2013): Chrysotile dissolution rates: implications for carbon sequestration; Applied Geochemistry, v. 35, p. 244–254.

Vanderzee, S.S.S., Power, I.M., Dipple, G.M. and Bradshaw, P.M.D. (2018): Carbon mineralization in ultramafic tailings, central British Columbia: a prospect for stabilizing mine waste and reducing greenhouse gas emissions; *in* Geoscience BC Summary of Activities 2017: Minerals and Mining, Geoscience BC, Report 2018-1, p. 109–112.

Wilson, S.A., Raudsepp, M. and Dipple, G.M. (2006): Verifying and quantifying carbon fixation in minerals from serpentine-rich mine tailings using the Rietveld method with X-ray powder diffraction data; American Mineralogist, v. 91, p. 1331–1341.

Wilson, S.A., Harrison, A.L., Dipple, G.M., Power, I.M., Barker, S.L.L., Mayer, K.U., Fallon, S.J., Raudsepp, M. and Southam, G. (2014): Offsetting of CO_2 emissions by air capture in mine tailings at the Mount Keith Nickel Mine, Western Australia: rates, controls and prospects for carbon neutral mining; Journal of Greenhouse Gas Control, v. 25, p. 121–140.

WMC Resources Ltd. (2002): WMC Resources Ltd Sustainability Report 2002; WMC Resources Ltd., URL <https://www.bhp.com/-/media/bhp/documents/investors/reports/2002/wmcsustainability2002.pdf?la=en> [November 2018].

Worrell, E., Price, L., Martin, N., Hendriks, C. and Meida, L.O. (2001): Carbon dioxide emissions from the global cement industry; Annual Review of Energy and the Environment, v. 26, p. 303–329, URL <https://doi.org/10.1146/annurev.energy.26.1.303> [November 2018].